

Probing scalar, Dirac, Majorana and vector DM through spin-0 electron-specific mediator at the electron fixed-target experiments

I. V. Voronchikhin^{1,*} and D. V. Kirpichnikov^{2,†}

¹*Tomsk Polytechnic University, 634050 Tomsk, Russia*

²*Institute for Nuclear Research, 117312 Moscow, Russia*

(Dated: December 27, 2023)

We discuss the thermal target curves of Majorana, Dirac, scalar and vector light dark matter (DM) that are associated with the freeze-out mechanism via the annihilation into e^+e^- pair through the electron-specific spin-0 mediator of dark matter. We also discuss the mechanism to produce the regarding DM mediator in the electron (positron) fixed-target experiments such as NA64e and LDMX. We derive the corresponding experimental reaches of the NA64e and LDMX that are complementary to the DM thermal target parameter space.

I. INTRODUCTION

A significant number of astrophysical observations lead to the hypothesis of dark matter (DM), that manifests itself via the gravitational effects (for a review see e. g. Refs. [1, 2]). However, the nature of DM particles still remains of the great interest, despite the overwhelming evidences of indirect observation. Moreover, 85 % of the total amount of matter [3] in the Universe is approximately invisible and that motivates a development of extension of the Standard model (SM). In addition, DM particles can solve other well-known problems of modern physics, for instance the anomalous magnetic moment puzzle [4].

The gravitational evidences cannot directly specify the range of DM particle masses that can span a significant orders of magnitude leading to different cosmological consequences. However, if DM particles achieve thermalization with SM particles in the thermal bath of the early Universe, the range of viable masses decreases. In particular, DM masses below a few keV are too hot for structure formation and DM masses above 100 TeV are in tension with perturbative unitarity [5]. The expansion of the Universe results in DM freeze-out that leads to its decoupling and the relic abundance. It is worth mentioning that thermal freeze-out is relatively insensitive to initial conditions of the early Universe [6, 7].

Thermal contact between DM and SM particles lead to overproduction of DM particles in the early Universe, therefore the relic abundance requires a depletion mechanism to yield the observed value [5]. Further, the assumption of the weak interaction between DM and SM particles lead to weak interacting massive particle (WIMP) that takes masses in the Lee-Weinberg bounds [8, 9] from few GeV to 100 TeV. However, the heavy range of WIMP masses is ruled out by the direct detection experiments [10–12] that motivates the search of light DM in the sub-GeV mass region. To avoid the DM overproduction one

can suggest the scenario with the mediator of DM (MED) that can connect light DM and SM particles via portals.

In particular, the typical scenarios and the regarding thermal target associated with dark boson mediators include spin-0, spin-1 and spin-2 particles such as the hidden Higgs boson [13–19], the dark photon [20–32], and the dark graviton [33–45], respectively. Also, in the mass range of light DM from few MeV to GeV the fixed-target experiments combine the advantages of high-energy particle beam and its relative large intensity.

In this paper, we focus on DM in the mass range between $\mathcal{O}(1)$ MeV and $\mathcal{O}(1)$ GeV. In the following we consider the DM parameter space with a typical branching fraction of the scalar electron-specific mediator $\text{Br}(\text{MED} \rightarrow \text{DM DM}) \simeq 1$, that implies the condition for the masses $2m_{\text{DM}} \lesssim m_{\text{MED}}$. We consider several simplified scenarios with specific DM types such as Majorana, Dirac, scalar and vector particles. Moreover, we use effective interactions of electron-specific scalar MED that can be potentially coupled with SM particles via singlet extension of the Higgs sector. We calculate a new constraint on the coupling between the scalar MED and a electron by using the null-results of fixed-target experiments such as NA64e and LDMX. We also show the complementarity of the derived bounds to the thermal target curves of the specific DM type. We pay additional attention to the resonant annihilation of electron-positron pair into DM via the scalar MED that also provides a new constraint on the light DM parameter space from NA64e and LDMX.

This paper is organized as follows. In Sec. II we describe the benchmark scenarios for the electron-specific scalar MED. In Sec. III we briefly provide the procedure for the calculation of relic density of DM for the simplified models. In Sec. IV we discuss the missing energy signal and review the main benchmark parameters of electron fixed-target facilities. In Sec. V we derive explicitly the decay widths of scalar mediator and the resonant cross sections of the process $e^+e^- \rightarrow \phi \rightarrow \text{DM} + \text{DM}$ at NA64e and LDMX. In Sec. VI we obtain the thermal target curves of various types of DM. In Sec. VII we discuss the experimental reach of NA64e and LDMX for the the specific light DM parameter space. We conclude in

* e-mail: i.v.voronchikhin@gmail.com

† e-mail: dmbrick@gmail.com

Sec. VIII.

II. BENCHMARK SCENARIOS

In this section we discuss simplified benchmark DM scenarios focusing on the electron-specific scalar mediator interacting with scalar, Dirac, Majorana, and vector DM. By diagonalizing the mass terms after the electroweak symmetry breaking in the effective field theory [5, 46, 47] one can obtain the coupling between SM particles and the scalar MED.

To be more concrete we consider four types of the effective Lagrangians involving scalar MED ϕ , electron e and the specific types of DM

$$\mathcal{L}_{\text{eff}}^S \supset \frac{1}{2} c_{SS}^\phi \phi S^2 + c_{ee}^\phi \phi \bar{e} e, \quad (1)$$

$$\mathcal{L}_{\text{eff}}^\psi \supset c_{\psi\psi}^\phi \phi \bar{\psi} \psi + c_{ee}^\phi \phi \bar{e} e, \quad (2)$$

$$\mathcal{L}_{\text{eff}}^\chi \supset \frac{1}{2} c_{\chi\chi}^\phi \phi \bar{\chi} \chi + c_{ee}^\phi \phi \bar{e} e, \quad (3)$$

$$\mathcal{L}_{\text{eff}}^V \supset \frac{1}{4} c_{VV}^\phi \phi V^{\mu\nu} \tilde{V}_{\mu\nu} + c_{ee}^\phi \phi \bar{e} e, \quad (4)$$

where c_{SS}^ϕ , $c_{\psi\psi}^\phi$, $c_{\chi\chi}^\phi$, c_{VV}^ϕ are coupling constants for real scalar DM S [46], Dirac fermion DM ψ [5, 48], Majorana fermion χ [46, 49] and vector DM V_μ [50–53] with the spin-0 mediator, respectively, c_{ee}^ϕ is the constant of coupling between the scalar MED and the electron [26, 49], $V^{\mu\nu}$ is the field strength tensor, $\tilde{V}_{\mu\nu} = 1/2 \epsilon^{\mu\nu\alpha\beta} V_{\alpha\beta}$ is the dual field strength tensor.

It is worth noticing that for the Majorana DM we employ the 4-component spinor formalism [54]. We introduce an ubiquitous in a literature notations for the couplings

$$(\epsilon_{ee}^\phi)^2 = (c_{ee}^\phi)^2 / (4\pi\alpha), \quad \alpha_{\text{DM}} = (c_{\text{DM}}^\phi)^2 / (4\pi), \quad (5)$$

where α_{DM} and $\alpha \approx 1/137$ are the dark and electromagnetic fine structure constants, respectively. For concreteness we also assume throughout the paper that the visible decays of mediator $\phi \rightarrow e^+ e^-$ are subdominant with respect to the invisible $\phi \rightarrow \text{DM} + \text{DM}$, such that its DM branching fraction is dominant, $\text{Br}(\phi \rightarrow \text{DM} + \text{DM}) \simeq 1$.

III. RELIC ABUNDANCE

In this section we discuss in detail the procedure of calculation for the relic abundance of DM due to the annihilation freeze-out reaction $p_1^{\text{DM}} + p_2^{\text{DM}} \rightarrow p_a^{\text{SM}} + p_b^{\text{SM}}$. The Boltzmann equation can be written by defining the term $Y(x) = n(x)/s(x)$ as a ratio of DM number density $n(x)$ over the SM entropy density $s(x)$ in the following form:

$$\frac{dY}{dx} = -Q(x) (Y^2(x) - Y_{\text{eq}}^2(x)), \quad Y_{\text{eq}}(x) = \frac{n_{\text{eq}}(x)}{s(x)}, \quad (6)$$

where $x = m_{\text{DM}}/T$, T is the typical temperature, $n_{\text{eq}}(x)$ is the density of particle number in the thermal equilibrium. The function $Q(x)$ and the total entropy density s read, respectively:

$$Q(x) = \frac{c s(m_{\text{DM}})}{H(m_{\text{DM}})} \langle \sigma v_{\text{Mol}} \rangle, \quad s(T) = \frac{2\pi^2}{45} g_{*s}(T) T^3, \quad (7)$$

where $g_{*s}(T)$ is the entropy effective degree of freedom [55]. The coefficient is chosen to be $c = 1$ for the case when DM is its own antiparticle (Majorana fermion, scalar and vector types of DM), and $c = 1/2$ for the opposite case (i. e. for the Dirac fermion DM) [56]. The Hubble parameter is defined as [57]:

$$H(x) \simeq \frac{H(m_{\text{DM}})}{x^2}, \quad H(m_{\text{DM}}) \simeq 0.331 g_{*s}^{1/2}(m_{\text{DM}}) \frac{m_{\text{DM}}^2}{M_{\text{Pl}}},$$

where $M_{\text{Pl}} \simeq 2.4 \cdot 10^{18}$ GeV is the reduced Planck mass, $g_{*s}(T)$ is the energy effective degree of freedom [55], $\langle \sigma v_{\text{Mol}} \rangle$ is the thermal averaged cross section for a reaction $2 \rightarrow 2$ that is given by [58]:

$$\langle \sigma v_{\text{Mol}} \rangle = \frac{\int \sigma v_{\text{Mol}} e^{-E_1/T} e^{-E_2/T} d^3 \mathbf{p}_1 d^3 \mathbf{p}_2}{\int e^{-E_1/T} e^{-E_2/T} d^3 \mathbf{p}_1 d^3 \mathbf{p}_2}, \quad (8)$$

where $p_1^{\text{DM}} = (E_1, \mathbf{p}_1)$, $p_2^{\text{DM}} = (E_2, \mathbf{p}_2)$ are 4-momenta of DM, v_{Mol} is the Moller velocity [59]:

$$v_{\text{Mol}} = \frac{\sqrt{\lambda(s, m_1^2, m_2^2)}}{2E_1 E_2}, \quad (9)$$

and $\lambda(s, m_1^2, m_2^2) = (s - (m_1 + m_2)^2)(s - (m_1 - m_2)^2)$ is the triangle function. The expressions for the total cross section of the DM annihilation σ are provided explicitly in Sec. VI for the specific DM type. In the expression of thermal average of cross section (8) we neglect the chemical potential and assume the Maxwell-Boltzmann distribution for the particle species.

The decoupling of the considered type of particles is achieved if the following condition is fulfilled:

$$c n_{\text{eq}}(x_f) \langle \sigma v_{\text{Mol}} \rangle|_{x=x_f} \simeq H(x_f), \quad (10)$$

where T_f is the critical temperature and $x_f = m_{\text{DM}}/T_f$ is the parameter of freeze-out. The current value of variable Y tends to the relic value $Y(\infty)$, that can be estimated on the interval (x_f, ∞) from the Boltzmann equation (6) as:

$$Y^{-1}(\infty) = \frac{c s(m_{\text{DM}})}{H(m_{\text{DM}})} J(x_f), \quad J(x_f) = \int_{x_f}^{\infty} \frac{\langle \sigma v_{\text{Mol}} \rangle}{x^2} dx, \quad (11)$$

where we take into account that $Y(x) \gg Y_{\text{eq}}(x)$ for $x > x_f$. In case of s-wave annihilation one can exploit $J(x_f) = \langle \sigma v_{\text{Mol}} \rangle / x_f$. Next, from the Friedmann equations for the critical density of the DM one can obtain that

$$\Omega_{\text{DM}} \simeq \frac{m_{\text{DM}} s_0 Y(\infty)}{3 M_{\text{Pl}}^2 H_0^2}, \quad (12)$$

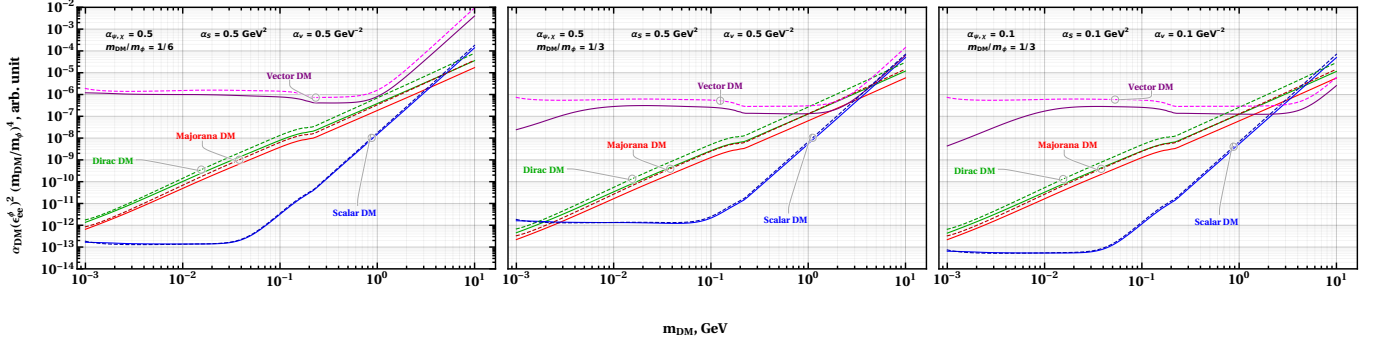


Figure 1. The relic DM thermal target curves as a function of mass for Majorana DM (red line), Dirac DM (green line), vector DM (purple line) and scalar DM (blue line) that annihilate via scalar MED. Solid lines correspond to the numerical calculation through integral (14) and the dashed lines are associated with semi-analytical calculation of the thermal target in the low-velocity approach (16). Left panel: relic thermal targets for $\alpha_{\text{DM}} = 0.5$ ($\text{GeV}^2/\text{GeV}^{-2}$) and $m_{\text{DM}}/m_\phi = 1/6$. Center panel: relic targets for $\alpha_{\text{DM}} = 0.5$ ($\text{GeV}^2/\text{GeV}^{-2}$) and $m_{\text{DM}}/m_\phi = 1/3$. The right panel: relic targets for $\alpha_{\text{DM}} = 0.1$ ($\text{GeV}^2/\text{GeV}^{-2}$) and $m_{\text{DM}}/m_\phi = 1/3$.

where $s_0 = s(T_0)$, $T_0 = 2.35 \cdot 10^{-13}$ GeV are the current total entropy density and temperature of the Universe, $H_0 = 2.13 h \cdot 10^{-42}$ GeV is the current value of the Hubble parameter with the dimensionless constant $h \simeq 0.674 \pm 0.005$ [3]. As a result, the expression of relic density takes the following form [34, 57, 60]:

$$\Omega_c h^2 \simeq 0.85 \cdot 10^{-10} g_{*s}^{-1/2} (m_{\text{DM}}) \frac{1}{c} \left(\frac{J(x_f)}{\text{GeV}^{-2}} \right)^{-1}, \quad (13)$$

where it is taken into account that $g_{*s}(T_0) \approx 3.91$ and for $T \gtrsim 1$ MeV we can set $g_{*s}(T) \simeq g_{*s}(T)$. In addition, we take into account that the current value of relic abundance of cold DM obtained from the Planck 2018 combined analysis is [3]:

$$\Omega_c h^2 = 0.1200 \pm 0.0012.$$

Moreover, assuming s-wave annihilation one can see from the relic density (13) that the typical value of thermal averaged cross section is evaluated as $\langle \sigma v_{\text{Mol}} \rangle \simeq 2.5 \times 10^{-9} \text{ GeV}^{-2} \approx 3 \times 10^{-26} \text{ cm}^3 \text{ s}^{-1}$ [40, 61] where we imply that $c = 1$ and the typical parameters are $m_{\text{DM}} \simeq \mathcal{O}(10)$ MeV, $g_{*s} \simeq \mathcal{O}(10)$ and $x_f \simeq \mathcal{O}(10)$. Next, using the direct integration of expression (8), the thermal averaged cross section for $x \gtrsim 1/3$ can be written as [5, 58, 62]:

$$\langle \sigma v_{\text{Mol}} \rangle \simeq \int_{4m_{\text{DM}}^2}^{\infty} \sigma(s) \frac{\lambda(s, m_{\text{DM}}^2, m_{\text{DM}}^2)}{N_{\langle \sigma v_{\text{Mol}} \rangle} \sqrt{s}} K_1 \left(\frac{\sqrt{s}}{T} \right) ds, \quad (14)$$

$$N_{\langle \sigma v_{\text{Mol}} \rangle} = 8T m_{\text{DM}}^4 (K_2(m_{\text{DM}}/T))^2, \quad (15)$$

where $K_i(z)$ is the modified Bessel functions of the second kind of i^{th} order [63]. Also, we use the critical temperature $T_f = m_{\text{DM}}/20$ [5, 8] for the calculation of relic abundance with the integral (14).

A. Low-velocity approach

By using the velocity expansion for the thermal averaged of cross section in the non-relativistic approach one can get [58, 64]:

$$\langle \sigma v_{\text{Mol}} \rangle = \frac{1}{2\sqrt{\pi}} \sum_{k=0}^{\infty} 4^{k+1} \Gamma(k+3/2) \frac{a_k}{k!} x^{-k} \approx a_0 + 6a_1 x^{-1} + 30a_2 x^{-2}, \quad (16)$$

where $\Gamma(k)$ is the Gamma function, a_k are the expansion coefficients of cross section for the low-velocity series. Indeed, the low-velocity approach is possible due to the angular independence of Mandelstam variables in the zero velocity [65]. As a result, for the calculation of relic density one can use a first non-zero term in the low-velocity approach as $\langle \sigma v_{\text{Mol}} \rangle = \sigma_0 x^{-n}$. It is worth mentioning that $n = 0$, $n = 1$ and $n = 2$ correspond to the s-wave, p-wave and d-wave annihilations, respectively [57]. Hence, by taking into account the condition of decoupling (10) and the relic density (12) one can get final expressions for a calculation of relic abundance in the low-velocity approach [57, 60]:

$$\langle \sigma v_{\text{Mol}} \rangle = (c_{ee}^\phi)^2 \sigma_0 x^{-n}, \quad (17)$$

$$x_f = \ln \left((c_{ee}^\phi)^2 \sigma_0 \frac{3\sqrt{5} M_{\text{Pl}}}{2\pi^{5/2}} \frac{g_i m_{\text{DM}}}{\sqrt{g_{*s}(m_{\text{DM}})}} \right), \quad (18)$$

$$\Omega_c h^2 = \frac{0.85 \cdot 10^{-10}}{c(c_{ee}^\phi)^2} \frac{(n+1)x_f^{n+1}}{g_{*s}^{1/2}(m_{\text{DM}})\sigma_0} \text{ GeV}^{-2}, \quad (19)$$

where g_i - the internal degrees of freedom, n is the first non-zero power in the low-velocity series.

The calculation of relic density is associated with the Eqs. (18) and (19) for c_{ee}^ϕ and x_f in case of low-velocity approximation. Opposite, we have the direct expression for parameters c_{ee}^ϕ with $x_f = \text{const}$ in case using the integral formula for the thermal average of cross section

(14). Indeed, in case of low-velocity approximation the relic density depends polynomially on the freeze-out parameter and this system can be analytically solved for x_f and c_{ee}^ϕ .

IV. MISSING ENERGY SIGNAL

In this section we discuss the electron missing energy signatures and the typical parameters of the NA64e and LDMX experiments for probing DM mediators.

We estimate the number of MEDs produced due to the bremsstrahlung for fixed-target facilities as follows:

$$N_{\text{MED}}^{\text{brem.}} \simeq \text{EOT} \cdot \frac{\rho N_A}{A} L_T \int_{x_{\min}}^{x_{\max}} dx \frac{d\sigma_{2 \rightarrow 3}(E_0)}{dx} \eta_{\text{MED}}^{\text{brem.}}, \quad (20)$$

where L_T is the effective interaction length of the electron in the target, EOT is a number of electrons accumulated on target, ρ is the target density, N_A is Avogadro's number, A is the atomic weight number, Z is the atomic number, $\eta_{\text{MED}}^{\text{brem.}}$ is a typical efficiency for the bremsstrahlung emission of the MED, $d\sigma_{2 \rightarrow 3}/dx$ is the differential cross section of the electron missing energy process $eN \rightarrow eN\phi$ [66, 67], $E_0 \equiv E_{\text{beam}}$ is the initial energy of electron beam, x_{\min} and x_{\max} are the minimal and maximal fraction of missing energy, respectively, for the experimental setup, $x \equiv E_{\text{miss}}/E_0$, where $E_{\text{miss}} \equiv E_{\text{MED}}$.

Also, the typical number of hidden bosons produced due to the annihilation is estimated to be:

$$N_{\text{MED}}^{\text{ann.}} \simeq \text{EOT} \frac{\rho N_A Z L_T}{A} \int_{E_{e^+}^{\text{cut}}}^{E_{e^+}^{\text{max}}} dE_{e^+} \sigma_{\text{tot}}(E_{e^+}) T(E_{e^+}) \eta_{\text{MED}}^{\text{ann.}}, \quad (21)$$

where $\sigma_{\text{tot}}(E_{e^+})$ is the resonant total cross section of the electron-positron annihilation into DM (see Sec. V below), $\eta_{\text{MED}}^{\text{ann.}}$ is a typical efficiency associated with MED production via the resonant channel (we conservatively imply throughout the paper that signals for both positron and electron beam modes have the same efficiency $\eta_{\text{MED}}^{\text{ann.}}$), E_{e^+} is the energy of secondary positrons, $E_{e^+}^{\text{cut}} = E_0 x_{\min}$ and $E_{e^+}^{\text{max}} = E_0$ are the minimal and maximal energies of secondary positrons in the electromagnetic shower, respectively.

A. Positron track-length distribution

In this subsection we briefly discuss the using positron track-length distribution in a target due to the electromagnetic shower development from the incoming primary electron or positron beams.

The analytical approximation for the typical differential positron track-length distribution $T(E_{e^+})$ was studied in detail [68–72]. For the thick target it was shown that $T(E_{e^+})$ depends, at first order, on a specific

type of target material through the multiplicative factor $T(E_{e^+}) \propto X_0$, where X_0 is the radiation length. Moreover, $T(E_{e^+})$ depends also on the ratio E_{e^+}/E_0 , where E_0 is the energy of the primary impinging particle. This allows to exclude the dependence on the energy of the primary beam and radiation length. As a result, we can get the universal distribution of positrons [66, 72, 73] adapted from Refs. [73, 74] that is characterized by the energy of primary beam E_0 and the target material X_0 of the NA64e experiment. For the electromagnetic shower development of positrons we use numerical Monte Carlo simulations in GEANT4 [75]. It is important to mention that the dependence of typical angles between the primary beam direction and a momentum of the secondary positrons can be neglected [72].

B. Fixed-target experimental setup

In this subsection we briefly summarize the benchmark parameters of the NA64e and LDMX electron fixed-target experiments that are exploited to constrain the parameter space of DM.

In case of fixed-target experiments with the initial energy of electron beam E_0 , the fraction of the primary beam energy $E_{\text{miss}} = xE_0$ can be carried away by a DM pair, that passes the detector of experiment without the energy deposition. The remaining part of the beam energy fraction, $E_e^{\text{rec}} \simeq (1 - x)E_0$, can be deposited in the active thick target by the recoil electrons (positrons). The fixed-target experiments allow investigating the relic DM with the mass in the range between 1 MeV and 1 GeV. It is worth mentioning that both NA64e and LDMX experiments have background suppression at the level of $\lesssim \mathcal{O}(10^{-13} - 10^{-12})$.

NA64e: the NA64e is the fixed-target experiment located at CERN North Area with a beam from the Super Proton Synchrotron (SPS) H4 beamline. The ultrarelativistic electrons with the energy of $E_0 \simeq 100$ GeV can be exploited as the primary beam that is scattering off nuclei of an active thick target. The typical scheme of the NA64e setup, the detector equipment and event selection rules can be found elsewhere in Ref. [74, 76, 77]. The efficiencies $\eta_{\text{MED}}^{\text{brem.}}$ and $\eta_{\text{MED}}^{\text{ann.}}$ are taken to be at the level of 90% for both electron and positron beam modes [74]. In case of NA64e experiment we use the following benchmark parameters ($\rho \simeq 11.34$ g cm $^{-3}$, $A = 207$ g mole $^{-1}$, $Z = 82$, $X_0 = 2.56$ cm), the effective interaction length of the electron is $L_T = X_0$ and the missing energy fraction cut is $x_{\min} = 0.5$. In this work we also perform the analysis of the sensitivity of NA64e to probe DM for the accumulated data at the level of $\text{EOT} \simeq 9.37 \times 10^{11}$ (see e. g. Ref. [77] for detail).

The light dark matter experiment (LDMX): the LDMX is the projected electron fixed-target facility at Fermilab. The schematic layout and the rules for the missing momentum event selection of the LDMX experiment are given in Ref. [49]. The projected LDMX facility

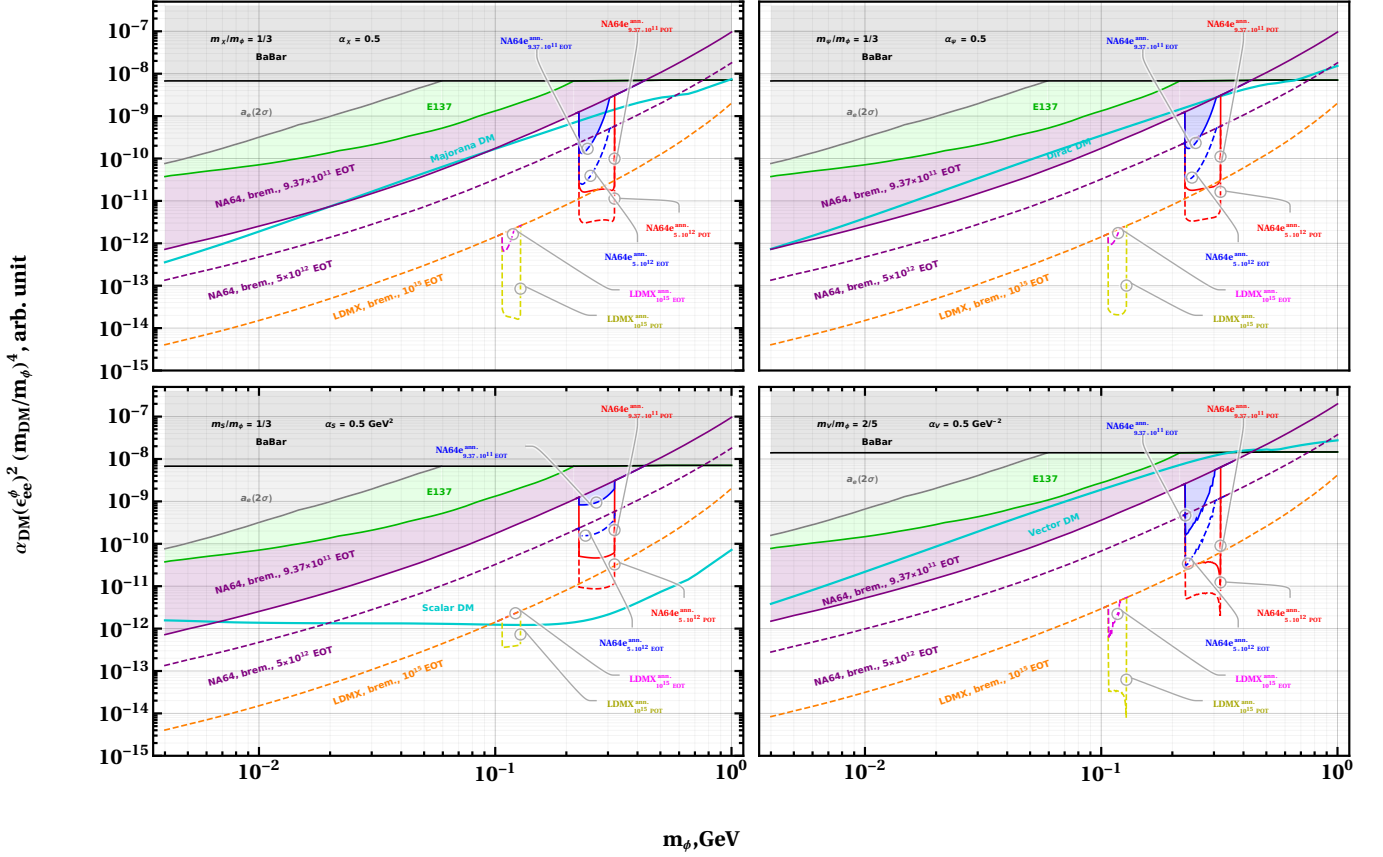


Figure 2. The experimental reach at 90 % C.L. as the function of MED mass for the NA64e and LDMX fixed-target facilities due to the ϕ -strahlung and resonant positron annihilation $e^+e^- \rightarrow \phi$, followed by the invisible decay $\phi \rightarrow \chi\chi$. For the calculation of relic thermal target we use numerical integration of (14). Grey shaded region corresponds to the existing BaBar [78] monophoton limit $e^+e^- \rightarrow \gamma\phi$. Green shaded region is the current reach of the electron beam dump E137 [25, 49, 79] experiment. The solid purple line corresponds to the existing NA64e limits for EOT $\simeq 9.37 \times 10^{11}$ from missing energy process $eN \rightarrow eN\phi$, the dashed purple line shows the expected limit for projected statistics EOT $\simeq 5 \times 10^{12}$. The solid blue line is the existing limit of the NA64e (EOT $\simeq 9.37 \times 10^{11}$) due to the positron annihilation mode $e^+e^- \rightarrow \phi$ with the primary e^- beam, the solid red line is the projected expected reach of NA64e for the positron annihilation channel with primary e^+ beam that corresponds to the 9.37×10^{11} positrons accumulated on target. Dashed blue and red lines correspond to the projected NA64e statistics 5×10^{12} of the annihilation mode $e^+e^- \rightarrow \phi$ for the e^- and e^+ primary beam, respectively. Dashed orange line is the projected LDMX limits for EOT $\simeq 10^{15}$ from the ϕ -strahlung process $eN \rightarrow eN\phi$. Dashed pink and yellow lines correspond to the projected LDMX statistics 10^{15} of the annihilation mode $e^+e^- \rightarrow \phi$ for the e^- and e^+ primary beam, respectively. Top Left, top right and bottom left panels correspond relic target for the Majorana, Dirac and scalar DM with parameters $\alpha_{DM} = 0.5 (\text{GeV}^2)$ and $m_{DM}/m_\phi = 1/3$. The bottom right panel corresponds the relic target for the vector DM with parameters $\alpha_V = 0.5 \text{ GeV}^{-2}$ and $m_{DM}/m_\phi = 2/5$.

would employ the unique electron missing momentum technique [80] that is complementary to the NA64e facility. The typical efficiencies η_{MED}^{brem} and η_{MED}^{ann} are estimated to be at the level of $\simeq 50\%$ for both electron [81] and positron beam options. Thus, for the LDMX experiment we employ the following benchmark parameters ($\rho = 2.7 \text{ g cm}^{-3}$, $A = 27 \text{ g mole}^{-1}$, $Z = 13$, $x_{min} = 0.7$, $X_0 = 8.9 \text{ cm}$) and $L_T \simeq 0.4 X_0 \simeq 3.56 \text{ cm}$. The typical efficiencies η_{MED}^{brem} and η_{MED}^{ann} are estimated to be at the level of $\simeq 50\%$ for both electron [81] and positron beam options. The energy of the primary beam is chosen to be $E_0 \simeq 16 \text{ GeV}$ and the projected moderate statistics corresponds to EOT $\simeq 10^{15}$ (it is planned however

to collect EOT $\simeq 10^{16}$ by the final phase of experimental running after 2027, see e. g. Ref. [81] and references therein for detail).

V. THE RESONANT DM PRODUCTION MECHANISM

In this section we provide a cross sections and widths of decay in case of scalar MED that are used for to constrain the coupling between the scalar MED and the electron. In the following we use an notations for typical velocities

and the inversed propagator squared:

$$\beta_{\text{DM}}(s) = \sqrt{1 - 4m_{\text{DM}}^2/s}, \quad \beta_e(s) = \sqrt{1 - 4m_e^2/s}, \quad (22)$$

$$D_{\text{DM}}^2(s) = (s - m_\phi^2)^2 + m_\phi^2(\Gamma_{\text{DM}}^{\text{tot}})^2. \quad (23)$$

For the calculation of both the decay width and cross section we employ the state-of-the-art FeynCalc package [82, 83] for the Wolfram Mathematica routine [84].

As we discussed above, the scalar mediator ϕ can be produced in the bremsstrahlung-like reaction $eN \rightarrow eN\phi$ followed by the invisible decay $\phi \rightarrow \text{DM} + \text{DM}$. The details of bremsstrahlung-like production of scalar MED in fixed-target experiments can be found elsewhere in Refs. [66, 67].

The widths of decay of the scalar MED into vector [52], Dirac fermion [5, 48], Majorana fermion [46], scalar [46] DM, and electron-positron pair read, respectively, as follows:

$$\Gamma_{\phi \rightarrow VV} = \frac{1}{2} \cdot \frac{4\pi\alpha_V m_\phi^3}{32\pi} \beta_V^3(m_\phi^2), \quad (24)$$

$$\Gamma_{\phi \rightarrow \psi\bar{\psi}} = \frac{4\pi\alpha_\psi m_\phi}{8\pi} \beta_\psi^3(m_\phi^2), \quad (25)$$

$$\Gamma_{\phi \rightarrow \chi\chi} = \frac{1}{2} \cdot \frac{4\pi\alpha_\chi m_\phi}{8\pi} \beta_\chi^3(m_\phi^2), \quad (26)$$

$$\Gamma_{\phi \rightarrow SS} = \frac{1}{2} \cdot \frac{4\pi\alpha_S}{16\pi m_\phi} \beta_S(m_\phi^2), \quad (27)$$

$$\Gamma_{\phi \rightarrow e^+e^-} \simeq \frac{(c_{ee}^\phi)^2 m_\phi}{8\pi} \beta_e^3(m_\phi^2), \quad (28)$$

where we use conventions defined by Eq. (22). For the invisible mode we imply that $m_{\text{MED}} \gtrsim 2m_{\text{DM}}$ and $\Gamma_{\text{MED} \rightarrow e^+e^-} \ll \Gamma_{\text{MED} \rightarrow \text{DM DM}}$ throughout the paper and therefore it leads to the benchmark total decay widths $\Gamma_{\text{DM}}^{\text{tot}} \simeq \Gamma_{\text{MED} \rightarrow \text{DM DM}}$.

The resonant total cross sections in case scalar, Dirac, Majorana and vector DM read, respectively:

$$\sigma_{e^+e^- \rightarrow \phi \rightarrow SS} = \frac{1}{2} \frac{4\pi\alpha_S (c_{ee}^\phi)^2}{32\pi} \frac{\beta_S(s)\beta_e(s)}{D_S^2(s)}, \quad (29)$$

$$\sigma_{e^+e^- \rightarrow \phi \rightarrow \psi\bar{\psi}} = \frac{4\pi\alpha_\psi (c_{ee}^\phi)^2}{16\pi} \frac{s\beta_\psi^3(s)\beta_e(s)}{D_\psi^2(s)}, \quad (30)$$

$$\sigma_{e^+e^- \rightarrow \phi \rightarrow \chi\chi} = \frac{1}{2} \frac{4\pi\alpha_\chi (c_{ee}^\phi)^2}{16\pi} \frac{s\beta_\chi^3(s)\beta_e(s)}{D_\chi^2(s)}, \quad (31)$$

$$\sigma_{e^+e^- \rightarrow \phi \rightarrow VV} = \frac{1}{2} \frac{4\pi\alpha_V (c_{ee}^\phi)^2}{64\pi} \frac{s^2\beta_V^3(s)\beta_e(s)}{D_V^2(s)}, \quad (32)$$

where the Mandelstam invariant is $s = (p_{e^-} + p_{e^+})^2$. In case of fixed-target experiments, the high-energy primary electron or positron beams are incident on the fixed dump that entails the development of an electromagnetic shower inside the thick active target. Thus, secondary positrons from the electromagnetic shower can annihilate on atomic electrons of target material via scalar MED into DM. One can see that typical momenta of the atomic electrons and secondary positrons

are $p_{e^-} = (m_e, 0, 0, 0)$ and $p_{e^+} \simeq (E_{e^+}, 0, 0, E_{e^+})$, respectively, where are neglected the motion of atomic electrons. In addition, we focus only on ultrarelativistic positrons due to $m_e < m_{\text{DM}}$ in the mass region of light DM, therefore, $|p_{e^+}| \simeq E_{e^+}$. As a result, the invariant mass s takes the following expression:

$$s = m_e^2 + 2m_e E_{e^+} \simeq 2m_e E_{e^+}, \quad (33)$$

that is employed in Eqs. (29), (30), (31), (32), and (21) for the calculation of the resonant missing energy signal yield.

It is important to mention that the resonant total cross section of process $f\bar{f} \rightarrow R \rightarrow l\bar{l}$ can be calculated by the Breit-Wigner (BW) resonant formula [85, 86]:

$$\sigma_{f\bar{f} \rightarrow R \rightarrow l\bar{l}} = \frac{2J+1}{(2S_1+1)(2S_2+1)} \frac{16\pi C_{BW}}{(1-4m_f^2/s)} \frac{\Gamma_{\text{in}}(s)\Gamma_{\text{out}}(s)}{(s-m_R^2)^2 + m_R^2(\Gamma_{\text{DM}}^{\text{tot}})^2}, \quad (34)$$

where Γ_{tot} is a total width of decay of resonance, Γ_{in} , Γ_{out} are widths of decay of scalar MED in initial and final states, respectively, J is a spins of resonance, S_1 and S_2 are spins of initial particles, $C_{BW} = 1$ and $C_{BW} = 2$ for different and identical particles in the initial state, respectively, that compensates the additional factor in the decay width in the case of identical particles [87, 88].

By substituting the decay widths (24), (25), (26), (27), and (28) into the Breit-Wigner resonant formula (34) one can reproduce the result for the FeynCalc straightforward calculation of the total cross sections (29), (30), (31), and (32). That cross-check was used in order to validate our analytical calculations.

VI. THERMAL TARGET

In this subsection, we briefly discuss cross sections of DM annihilation into electron-positron pair via the scalar MED for different types of DM. We also plot regarding thermal target curves. In case of invisible decay mode the interaction can be realized via the s-channel. The resonant total cross sections in the case of scalar MED and Dirac, Majorana, scalar, vector DM read, respectively, as follows:

$$\sigma_{\psi\bar{\psi} \rightarrow \phi \rightarrow e^+e^-} = \frac{4\pi\alpha_\psi (c_{ee}^\phi)^2}{16\pi} \frac{s\beta_\psi(s)\beta_e^3(s)}{D_\psi^2(s)}, \quad (35)$$

$$\sigma_{\chi\chi \rightarrow \phi \rightarrow e^+e^-} = \frac{4\pi\alpha_\chi (c_{ee}^\phi)^2}{16\pi} \frac{s\beta_\chi(s)\beta_e^3(s)}{D_\chi^2(s)}, \quad (36)$$

$$\sigma_{SS \rightarrow \phi \rightarrow e^+e^-} = \frac{4\pi\alpha_S (c_{ee}^\phi)^2}{8\pi} \frac{\beta_S^{-1}(s)\beta_e^3(s)}{D_S^2(s)}, \quad (37)$$

$$\sigma_{VV \rightarrow \phi \rightarrow e^+e^-} = \frac{4\pi\alpha_V (c_{ee}^\phi)^2}{144\pi} \frac{s^2\beta_V(s)\beta_e^3(s)}{D_V^2(s)}, \quad (38)$$

where we use the dark fine structure constant (5) and (22).

In non-relativistic approximation, $s \simeq 4m_{\text{DM}}^2$, the typical product of cross section and velocity reads as follows:

$$v_{\text{Mol}} \sigma_{\chi\chi \rightarrow \phi \rightarrow e^+e^-} = \frac{4\pi\alpha_\chi (c_{ee}^\phi)^2 m_\chi^2 \beta_e^3 (4m_\chi^2)}{8\pi D_\chi^2 (4m_\chi^2)} v_{\text{Mol}}^2, \quad (39)$$

$$v_{\text{Mol}} \sigma_{\psi\bar{\psi} \rightarrow \phi \rightarrow e^+e^-} = \frac{4\pi\alpha_\psi (c_{ee}^\phi)^2 m_\psi^2 \beta_e^3 (4m_\psi^2)}{8\pi D_\psi^2 (4m_\psi^2)} v_{\text{Mol}}^2, \quad (40)$$

$$v_{\text{Mol}} \sigma_{SS \rightarrow \phi \rightarrow e^+e^-} = \frac{4\pi\alpha_S (c_{ee}^\phi)^2 \beta_e^3 (4m_S^2)}{4\pi D_S^2 (4m_S^2)}, \quad (41)$$

$$v_{\text{Mol}} \sigma_{VV \rightarrow \phi \rightarrow e^+e^-} = \frac{4\pi\alpha_V (c_{ee}^\phi)^2 m_V^4 \beta_e^3 (4m_V^2)}{18\pi D_V^2 (4m_V^2)} v_{\text{Mol}}^2, \quad (42)$$

where the Moller's velocity in the center of mass is defined by (9). One can see that vector DM, Majorana and Dirac fermion DM annihilate in a p-wave, however the scalar DM annihilates in a s-wave. As an additional cross-check of the Eqs. (39), (40), and (41) we reproduce the expressions for Majorana DM [46, 49], Dirac DM [5, 89] and scalar DM [46], implying that $D_{\text{DM}}^2(4m_{\text{DM}}^2) \simeq (4m_{\text{DM}}^2 - m_\phi^2)^2$ in the non-relativistic approach.

In Fig. 1 we show the thermal target curves of different DM types that annihilates into e^+e^- pair via the electron-specific scalar MED. We compare the numerical calculation of the thermal target via Eq. (14) and the analytical non-relativistic approximation defined by Eq. (16).

Remarkably that the numerical result for the thermal target curve coincides fairly well with the analytical one for the scalar DM that annihilates in a s-wave for the wide range of DM mass $1 \text{ MeV} \lesssim m_S \lesssim 10 \text{ GeV}$ far from the resonant point $m_\phi \gtrsim 3m_S$. It is worth noticing that for the fermionic DM (Dirac and Majorana), that annihilates in a p-wave, the discrepancy between analytical and numerical approach can be as large as $\gtrsim 20 \%$ for the mass range of interest $1 \text{ MeV} \lesssim m_{\psi,\chi} \lesssim 10 \text{ GeV}$ and $m_\phi \gtrsim 3m_{\psi,\chi}$. Moreover, the difference between thermal target curve of Dirac DM and Majorana DM can be explained due to the particle-antiparticle coefficient c (for details see e. g. discussion after Eq. (7)).

In order to cross-check our calculation, we reproduce the result of Ref. [49] for the Majorana thermal target curve associated with the electron-specific scalar mediator. For vector DM the analytical approach of low-velocity regime breaks at small DM masses $m_V \lesssim 10 \text{ MeV}$ and the regarding relative error can be relatively large for $m_\phi \simeq 3m_V$. This discrepancy is mitigated in the region far from the resonant point $m_\phi \simeq 6m_V$. In the following section, we rely on numerical approach for vector thermal target calculation [58, 64, 65].

VII. THE EXPERIMENTAL REACH

In this section we discuss current and expected experimental reach of the fixed-target facilities as NA64e and

LDMX for both primary electron and positron beams, implying that scalar mediator decays into the invisible mode. We use the typical number of signal events $N_{\text{sign.}} \gtrsim 2.3$ and obtain the 90% C. L. exclusion limit on the coupling constant between the electron and the scalar MED. Also, the background free case and the null-results of the missing energy events for both NA64e and LDMX experiments are used. Thus, for the signal yield that originates from MED-strahlung and e^+e^- annihilation into DM we put $N_{\text{sign.}} \simeq N_{\text{MED}}^{\text{brem.}} + N_{\text{MED}}^{\text{ann.}}$. In Fig. 2 we show the experimental reach of the NA64e and LDMX experiments.

We use the current statistics of NA64e as $\text{EOT} \simeq 9.37 \times 10^{11}$ and the projected statistics for NA64e and LDMX as $\text{EOT} \simeq 5 \times 10^{12}$ and $\text{EOT} \simeq 10^{15}$, respectively. We assume same statistics for both positron and electron primary beams in case of calculation of positron annihilation mode. We note that, for the e^+e^- annihilation mode, the projected positron beam provides a more stringent constraint on the electron-MED coupling than the electron primary beam bounds due to the presence of positrons in the first generation of the electromagnetic shower in the active target [66].

Remarkably, the NA64e experiment rules out the Dirac and vector DM for the currently accumulated statistics $\text{EOT} \simeq 9.37 \times 10^{11}$. In addition, the NA64e resonant enhancement of the exclusion limit in the mass range $0.23 \text{ GeV} \lesssim m_\phi \lesssim 0.32 \text{ GeV}$ and the bounds from ϕ -strahlung around $10^{-2} \text{ GeV} \lesssim m_\phi \lesssim 0.1 \text{ GeV}$ allow to exclude the Majorana DM. However, for the scalar DM the NA64e rules out only small part of relic thermal target parameter space below $m_\phi \lesssim 5 \times 10^{-3} \text{ GeV}$. Note that the LDMX can significantly constrain the electron-MED coupling due to the sufficiently large planned accumulated statistics.

VIII. CONCLUSION

In the present paper, we studied a sub-GeV range of simplified DM scenarios associated with the electron-specific scalar mediator and evaluated the sensitivity of electron fixed-target experiments such as NA64e and LDMX. In particular, we derived new constraints on the coupling of electrophilic scalar MED in case of e^+e^- annihilation mode and showed that these complement the bounds from the widely exploited ϕ -strahlung production, $eN \rightarrow eN\phi$, followed by the invisible decay, $\phi \rightarrow \text{DM} + \text{DM}$. In particular, the updated reach of NA64e and LDMX can be pushed down by a factor of $\mathcal{O}(1)$ for the specific range of light DM mass. We studied the different mechanism of DM production for the regarding experiments and showed that the resonant annihilation mode $e^+e^- \rightarrow \phi \rightarrow \text{DM} + \text{DM}$ can be a viable mechanism of the electron-specific MED production that provides an improved constraints for Majorana, Dirac, scalar and vector types of DM. We showed that NA64e rules out the typical parameter space of Majorana, Dirac

and vector DM for the specific set of benchmark parameters.

ACKNOWLEDGMENTS

We would like to thank A. Celentano, P. Crivelli, S. Demidov, R. Dusaev, S. Gninenko, D. Gorbunov, M. Kirsanov, N. Krasnikov, V. Lyubovitskij, L. Molina Bueno, A. Pukhov, A. Shevelev, H. Sieber, and A. Zhevlakov for very helpful discussions and correspondences. This work was supported by The Ministry of Science and Higher Education of the Russian Federation in part of the Science program (Project № FSWW-2023-0003)

-
- [1] L. Bergstrom, *Annalen Phys.* **524**, 479 (2012), arXiv:1205.4882 [astro-ph.HE].
 - [2] G. Bertone and D. Hooper, *Rev. Mod. Phys.* **90**, 045002 (2018), arXiv:1605.04909 [astro-ph.CO].
 - [3] N. Aghanim *et al.* (Planck), *Astron. Astrophys.* **641**, A6 (2020), [Erratum: *Astron. Astrophys.* 652, C4 (2021)], arXiv:1807.06209 [astro-ph.CO].
 - [4] T. Aoyama, *Physics Reports* **887**, 1 (2020), the anomalous magnetic moment of the muon in the Standard Model.
 - [5] G. Krnjaic, *Phys. Rev. D* **94**, 073009 (2016), arXiv:1512.04119 [hep-ph].
 - [6] L. J. Hall, K. Jedamzik, J. March-Russell, and S. M. West, *JHEP* **03**, 080 (2010), arXiv:0911.1120 [hep-ph].
 - [7] N. Brahma, S. Heeba, and K. Schutz, (2023), arXiv:2308.01960 [hep-ph].
 - [8] B. W. Lee and S. Weinberg, *Phys. Rev. Lett.* **39**, 165 (1977).
 - [9] E. W. Kolb and K. A. Olive, *Phys. Rev. D* **33**, 1202 (1986), [Erratum: *Phys. Rev. D* 34, 2531 (1986)].
 - [10] D. S. Akerib *et al.* (LUX), *Phys. Rev. Lett.* **118**, 021303 (2017), arXiv:1608.07648 [astro-ph.CO].
 - [11] E. Aprile *et al.* (XENON), *Phys. Rev. Lett.* **119**, 181301 (2017), arXiv:1705.06655 [astro-ph.CO].
 - [12] X. Cui *et al.* (PandaX-II), *Phys. Rev. Lett.* **119**, 181302 (2017), arXiv:1708.06917 [astro-ph.CO].
 - [13] J. McDonald, *Phys. Rev. D* **50**, 3637 (1994), arXiv:hep-ph/0702143.
 - [14] C. P. Burgess, M. Pospelov, and T. ter Veldhuis, *Nucl. Phys. B* **619**, 709 (2001), arXiv:hep-ph/0011335.
 - [15] J. D. Wells, *Perspectives on LHC Physics*, 283 (2008), arXiv:0803.1243 [hep-ph].
 - [16] R. M. Schabinger and J. D. Wells, *Phys. Rev. D* **72**, 093007 (2005), arXiv:hep-ph/0509209.
 - [17] G. Bickendorf and M. Drees, *Eur. Phys. J. C* **82**, 1163 (2022), arXiv:2206.05038 [hep-ph].
 - [18] E. E. Boos, V. E. Bunichev, and S. S. Trykov, (2022), arXiv:2205.07364 [hep-ph].
 - [19] H. Sieber, D. V. Kirpichnikov, I. V. Voronchikhin, P. Crivelli, S. N. Gninenko, M. M. Kirsanov, N. V. Krasnikov, L. Molina-Bueno, and S. Sekatskii, (2023), arXiv:2305.09015 [hep-ph].
 - [20] R. Catena and T. R. Gray, *JCAP* **11**, 058 (2023), arXiv:2307.02207 [hep-ph].
 - [21] B. Holdom, *Phys. Lett. B* **166**, 196 (1986).
 - [22] E. Izaguirre, G. Krnjaic, P. Schuster, and N. Toro, *Phys. Rev. Lett.* **115**, 251301 (2015), arXiv:1505.00011 [hep-ph].
 - [23] R. Essig, P. Schuster, N. Toro, and B. Wojtsekhowski, *JHEP* **02**, 009 (2011), arXiv:1001.2557 [hep-ph].
 - [24] Y. Kahn, G. Krnjaic, J. Thaler, and M. Tups, *Phys. Rev. D* **91**, 055006 (2015), arXiv:1411.1055 [hep-ph].
 - [25] B. Batell, R. Essig, and Z. Surujon, *Phys. Rev. Lett.* **113**, 171802 (2014), arXiv:1406.2698 [hep-ph].
 - [26] B. Batell, A. Freitas, A. Ismail, and D. Mckeen, *Phys. Rev. D* **98**, 055026 (2018), arXiv:1712.10022 [hep-ph].
 - [27] E. Izaguirre, G. Krnjaic, P. Schuster, and N. Toro, *Phys. Rev. D* **88**, 114015 (2013), arXiv:1307.6554 [hep-ph].
 - [28] A. Kachanovich, S. Kovalenko, S. Kuleshov, V. E. Lyubovitskij, and A. S. Zhevlakov, *Phys. Rev. D* **105**, 075004 (2022), arXiv:2111.12522 [hep-ph].
 - [29] V. E. Lyubovitskij, A. S. Zhevlakov, A. Kachanovich, and S. Kuleshov, *Phys. Rev. D* **107**, 055006 (2023), arXiv:2210.05555 [hep-ph].
 - [30] D. Gorbunov and D. Kalashnikov, *Phys. Rev. D* **107**, 015014 (2023), arXiv:2211.06270 [hep-ph].
 - [31] J. Claude, M. Dutra, and S. Godfrey, *Phys. Rev. D* **107**, 075006 (2023), arXiv:2208.09422 [hep-ph].
 - [32] W. Wang, W.-L. Xu, J. M. Yang, and R. Zhu, (2023), arXiv:2305.12668 [hep-ph].
 - [33] H. M. Lee, M. Park, and V. Sanz, *Eur. Phys. J. C* **74**, 2715 (2014), arXiv:1306.4107 [hep-ph].
 - [34] Y.-J. Kang and H. M. Lee, *The European Physical Journal C* **80** (2020), 10.1140/epjc/s10052-020-8153-x, arXiv:2001.04868.
 - [35] N. Bernal, M. Dutra, Y. Mambrini, K. Olive, M. Peloso, and M. Pierre, *Phys. Rev. D* **97**, 115020 (2018), arXiv:1803.01866 [hep-ph].
 - [36] M. G. Folgado, A. Donini, and N. Rius, *JHEP* **04**, 036 (2020), arXiv:1912.02689 [hep-ph].
 - [37] Y.-J. Kang and H. M. Lee, *Eur. Phys. J. C* **81**, 868 (2021), arXiv:2002.12779 [hep-ph].
 - [38] M. Dutra, *PoS LeptonPhoton2019*, 076 (2019), arXiv:1911.11844 [hep-ph].
 - [39] S. Clery, Y. Mambrini, K. A. Olive, A. Shkerin, and S. Verner, *Phys. Rev. D* **105**, 095042 (2022), arXiv:2203.02004 [hep-ph].
 - [40] H. M. Lee, M. Park, and V. Sanz, *JHEP* **05**, 063 (2014), arXiv:1401.5301 [hep-ph].
 - [41] J. A. Gill, D. Sengupta, A. G. and Williams, (2023), arXiv:2303.04329 [hep-ph].
 - [42] W. Wang, L. Wu, J. M. Yang, H. Zhou, and B. Zhu, *JHEP* **12**, 072 (2020), [Erratum: *JHEP* 02, 052 (2021)], arXiv:1912.09904 [hep-ph].

- [43] A. de Giorgi and S. Vogl, JHEP **11**, 036 (2021), arXiv:2105.06794 [hep-ph].
- [44] A. de Giorgi and S. Vogl, JHEP **04**, 032 (2023), arXiv:2208.03153 [hep-ph].
- [45] K. Jodłowski, (2023), arXiv:2305.05710 [hep-ph].
- [46] A. Djouadi, O. Lebedev, Y. Mambrini, and J. Quevillon, Phys. Lett. B **709**, 65 (2012), arXiv:1112.3299 [hep-ph].
- [47] O. Lebedev, H. M. Lee, and Y. Mambrini, Phys. Lett. B **707**, 570 (2012), arXiv:1111.4482 [hep-ph].
- [48] L. Marsicano, M. Battaglieri, A. Celentano, R. De Vita, and Y.-M. Zhong, Phys. Rev. D **98**, 115022 (2018), arXiv:1812.03829 [hep-ex].
- [49] A. Berlin, N. Blinov, G. Krnjaic, P. Schuster, and N. Toro, Phys. Rev. D **99**, 075001 (2019), arXiv:1807.01730 [hep-ph].
- [50] K. Kaneta, H.-S. Lee, and S. Yun, Phys. Rev. D **95**, 115032 (2017), arXiv:1704.07542 [hep-ph].
- [51] Y. Nomura and J. Thaler, Phys. Rev. D **79**, 075008 (2009), arXiv:0810.5397 [hep-ph].
- [52] K. Kaneta, H.-S. Lee, and S. Yun, Phys. Rev. Lett. **118**, 101802 (2017), arXiv:1611.01466 [hep-ph].
- [53] A. S. Zhevlakov, D. V. Kirpichnikov, and V. E. Lyubovitskij, Phys. Rev. D **106**, 035018 (2022), arXiv:2204.09978 [hep-ph].
- [54] H. K. Dreiner, H. E. Haber, and S. P. Martin, Phys. Rept. **494**, 1 (2010), arXiv:0812.1594 [hep-ph].
- [55] L. Husdal, Galaxies **4**, 78 (2016), arXiv:1609.04979 [astro-ph.CO].
- [56] M. Srednicki, R. Watkins, and K. A. Olive, Nucl. Phys. B **310**, 693 (1988).
- [57] E. W. Kolb and M. S. Turner, *The Early Universe*, Vol. 69 (1990).
- [58] P. Gondolo and G. Gelmini, Nucl. Phys. B **360**, 145 (1991).
- [59] M. Cannoni, Int. J. Mod. Phys. A **32**, 1730002 (2017), arXiv:1605.00569 [hep-ph].
- [60] Y. Kahn, G. Krnjaic, N. Tran, and A. Whitbeck, JHEP **09**, 153 (2018), arXiv:1804.03144 [hep-ph].
- [61] H. Cai, G. Cacciapaglia, and S. J. Lee, Phys. Rev. Lett. **128**, 081806 (2022), arXiv:2107.14548 [hep-ph].
- [62] A. Bharucha, F. Brümmer, N. Desai, and S. Mutzel, JHEP **02**, 141 (2023), arXiv:2209.03932 [hep-ph].
- [63] M. Abramowitz, I. A. Stegun, and R. H. Romer, *Handbook of mathematical functions with formulas, graphs, and mathematical tables* (American Association of Physics Teachers, 1988).
- [64] S.-M. Choi, H. M. Lee, and M.-S. Seo, JHEP **04**, 154 (2017), arXiv:1702.07860 [hep-ph].
- [65] J. D. Wells, (1994), arXiv:hep-ph/9404219.
- [66] I. V. Voronchikhin and D. V. Kirpichnikov, Phys. Rev. D **107**, 115034 (2023), arXiv:2304.14052 [hep-ph].
- [67] Y.-S. Liu, D. McKeen, and G. A. Miller, Phys. Rev. D **95**, 036010 (2017), arXiv:1609.06781 [hep-ph].
- [68] H. Bethe and W. Heitler, Proc. Roy. Soc. Lond. A **146**, 83 (1934).
- [69] J. F. Carlson and J. R. Oppenheimer, Phys. Rev. **51**, 220 (1937).
- [70] L. D. Landau, Proc. Roy. Soc. Lond. A **166** (1938), 10.1016/b978-0-08-010586-4.50041-9.
- [71] Y.-S. Tsai and V. Whitis, Phys. Rev. **149**, 1248 (1966).
- [72] L. Marsicano, M. Battaglieri, M. Bondi, C. D. R. Carvajal, A. Celentano, M. De Napoli, R. De Vita, E. Nardi, M. Raggi, and P. Valente, Phys. Rev. D **98**, 015031 (2018), arXiv:1802.03794 [hep-ex].
- [73] Y. M. Andreev *et al.*, Phys. Rev. D **104**, L091701 (2021), arXiv:2108.04195 [hep-ex].
- [74] Y. M. Andreev *et al.* (NA64), Phys. Rev. D **106**, 032015 (2022), arXiv:2206.03101 [hep-ex].
- [75] S. Agostinelli *et al.* (GEANT4), Nucl. Instrum. Meth. A **506**, 250 (2003).
- [76] Y. M. Andreev *et al.* (NA64), Phys. Rev. Lett. **129**, 161801 (2022), arXiv:2207.09979 [hep-ex].
- [77] Y. M. Andreev *et al.* (NA64), (2023), arXiv:2307.02404 [hep-ex].
- [78] J. P. Lees *et al.* (BaBar), Phys. Rev. Lett. **119**, 131804 (2017), arXiv:1702.03327 [hep-ex].
- [79] J. D. Bjorken, S. Ecklund, W. R. Nelson, A. Abashian, C. Church, B. Lu, L. W. Mo, T. A. Nunamaker, and P. Rassmann, Phys. Rev. D **38**, 3375 (1988).
- [80] J. Mans (LDMX), EPJ Web Conf. **142**, 01020 (2017).
- [81] T. Åkesson *et al.*, in *Snowmass 2021* (2022) arXiv:2203.08192 [hep-ex].
- [82] V. Shtabovenko, R. Mertig, and F. Orellana, Comput. Phys. Commun. **256**, 107478 (2020), arXiv:2001.04407 [hep-ph].
- [83] V. Shtabovenko, R. Mertig, and F. Orellana, Comput. Phys. Commun. **207**, 432 (2016), arXiv:1601.01167 [hep-ph].
- [84] W. R. Inc., “Mathematica, Version 13.1,” Champaign, IL, 2022.
- [85] R. L. Workman *et al.* (Particle Data Group), PTEP **2022**, 083C01 (2022).
- [86] Y. Cheng, S.-F. Ge, J. Sheng, and T. T. Yanagida, (2023), arXiv:2309.12043 [hep-ph].
- [87] A. I. L’vov, Phys. Atom. Nucl. **81**, 748 (2018).
- [88] H.-Y. Cheng, C.-W. Chiang, and C.-K. Chua, Phys. Rev. D **103**, 036017 (2021), arXiv:2011.07468 [hep-ph].
- [89] M. R. Buckley, D. Feld, and D. Goncalves, Phys. Rev. D **91**, 015017 (2015), arXiv:1410.6497 [hep-ph].